



**Please cite the Published Version**

Duncan, Oliver , Allen, Tom , Birch, Alana, Foster, Leon, Hart, John and Alderson, Andrew (2021) Effect of steam conversion on the cellular structure, Young's modulus and negative Poisson's ratio of closed cell foam. Smart Materials and Structures, 30 (1). 015031-015031. ISSN 0964-1726

**DOI:** <https://doi.org/10.1088/1361-665X/abc300>

**Publisher:** IOP Publishing

**Version:** Accepted Version

**Downloaded from:** <https://e-space.mmu.ac.uk/626695/>

**Usage rights:**  [Creative Commons: Attribution-Noncommercial-No Derivative Works 4.0](#)

**Additional Information:** This is an Author Accepted Manuscript of a paper accepted for publication in Smart Materials and Structures, published by and copyright IOP Publishing.

**Enquiries:**

If you have questions about this document, contact [openresearch@mmu.ac.uk](mailto:openresearch@mmu.ac.uk). Please include the URL of the record in e-space. If you believe that your, or a third party's rights have been compromised through this document please see our Take Down policy (available from <https://www.mmu.ac.uk/library/using-the-library/policies-and-guidelines>)

# Effect of steam conversion on the cellular structure, Young's modulus and negative Poisson's ratio of closed cell foam

*Olly Duncan<sup>1,2\*</sup>, Tom Allen<sup>1</sup>, Alana Birch<sup>1</sup>, Leon Foster<sup>3</sup>, John Hart<sup>3</sup>, Andrew Alderson<sup>2</sup>*

1. Department of Engineering, Manchester Metropolitan University, Manchester, UK
2. Materials and Engineering Research Institute, Sheffield Hallam University, Sheffield, UK
3. Advanced Wellbeing Research Centre, Sheffield Hallam University, Sheffield, UK

Corresponding author: [O.Duncan@mmu.ac.uk](mailto:O.Duncan@mmu.ac.uk)

**KEYWORDS:** Auxetic Closed Cell Foam, Steam Processing, Digital Image Correlation, Micro-Computed Tomography, Poisson's ratio, Young's Modulus

## **ABSTRACT**

Open cell auxetic foams have shown potential for use in sporting and other protective equipment. Previous conversion methods for auxetic closed cell foam used a bespoke pressure vessel. This work expands upon a recent method, using steam absorption followed by cooling and condensation, to change the cell shape of closed cell foam to impart a negative Poisson's ratio. Aiming to present a simple, repeatable conversion method, foam samples (20 x 10 x 100 mm)

floating in water filled ( $\sim 20^{\circ}\text{C}$ ), covered ceramic containers (300 x 200 x 100 mm) were heated in an oven at  $105^{\circ}\text{C}$  for between 1 and 6.5 hours. Based on the results for the smaller samples, a larger sample of foam (30 x 100 x 100 mm) was also converted, with a steaming time of 8 hours. Final volume ratio (original/final volume) increased with heating time, up to a maximum of 4.6. The amount and angle of re-entrant (inward folding) cell walls increased with final volume ratio as cells contracted further, evidenced by micro computed tomography. Poisson's ratios, measured using digital image correlation, were as low as -0.3 in tension and -1.1 in compression. Tensile Young's modulus increased from  $\sim 2$  MPa up to  $\sim 6$  MPa with final volume ratio and compressive Young's moduli reduced from  $\sim 1.5$  MPa for low values of final volume ratio between one and three, then remained close to 1.5 MPa.

## INTRODUCTION

The negative Poisson's ratio (NPR) of auxetic materials provides some enhanced and potentially beneficial characteristics, including; high indentation resistance [1,2], vibration damping [3], reduced peak forces under impact [4–7] and unique shape change [8]. Auxetic open cell foam has been suggested as an option to improve sporting impact protection [1,4,5,9–12], protective gloves for construction workers [3], prosthetic devices [13,14] and footwear [15]. Improving protective equipment, particularly helmets [16–19], back protectors [20–22] and running shoes [23,24], could help to reduce injuries, which place burdens on participants and national economies [25]. Wearers of prosthetic devices often report discomfort, despite developments in, mostly closed-cell foam, liners [26–28]. Auxetic structures are beginning to appear in commercial running shoes [29,30] and helmets [31,32].

There are established conversion methods for thermo-plastic auxetic open cell foams [10] (e.g. [33–41]). These conversions for open cell auxetic foam include thermo-mechanical [10] or thermo-

chemical methods [42,43], or a combination of both [7,43]. Compressing open cell foam into a mold, reducing volume by a factor of two to five, buckles cell ribs and imposes inward angled cell ribs, known as a re-entrant cellular structure [10,33,44]. Compression forming by vacuum bags and shaped molds can produce different shaped auxetic open cell foam sheets [45]. Thermal [10] or chemical [42,43] softening and re-hardening, through cooling or removal of the softening agent, fixes the imposed re-entrant cellular structure. Re-entrant cells can outwardly align in tension, or fold inward in compression, resulting in NPR [10,46]. Attempts to apply similar thermo-mechanical methods to closed cell foams have ruptured cell walls [33,47].

The Young's modulus of auxetic open cell foam is similar to that of conventional open cell foam; at  $\sim 0.02$  to  $0.20$  MPa [10,39,44]. Conventional open cell foam's cell ribs buckle beyond  $\sim 5\%$  compression, causing a plateau region in stress vs. strain relationships [39,44,46]. Auxetic open cell foams tend to have a quasi-linear compressive stress vs. strain relationship with a reduced plateau region [39,44,46]. Closed cell foams are stiffer (Young's moduli  $> 1$  MPa [9,20,28,48]) than open cell foam (Young's moduli  $\approx 0.02$  to  $0.20$  MPa [10,44,49,50]), as air cannot pass between cells, both before and after cell walls buckle at  $\sim 5\%$  compression [51,52]. Personal protective equipment [9,20,48], footwear [51,53–55] and prosthetic devices [26–28], where low thickness padding tends to be desirable, typically contains closed rather than open cell foam as the energy absorbing material.

Early conversions for closed cell auxetic foam that preserved cell walls used a pressure vessel to apply volumetric compression [56]; which is more complex than open cell auxetic foam conversions that typically use a simple metal mold and conventional oven [10,33–41]. The pressure vessel for fabricating closed cell auxetic foam [56] withstood heat ( $> 100$  °C) while

imposing pressures ( $> 350$  kPa) above the limits of many autoclaves ( $\sim 100$  kPa). A more recent, potentially simpler method [57], fabricated closed cell auxetic foam using a steam environment.

The steam processing method [57] first steamed closed cell polyethylene foams at  $100^{\circ}\text{C}$  for up to 10 hours. Upon cooling, steam absorbed by the foam condensed, producing a negative pressure differential that shrank samples and imparted a re-entrant cellular structure [57]. As the conversion temperature was close to the softening point of the polyethylene ( $\sim 110^{\circ}\text{C}$ ), the imposed structure was fixed after cooling [57]. Final volume ratios (FVR, original/final volume) between 1.3 and 6.0 were retained over time, and imparted Poisson's ratios were between -0.5 and 0.0. The work introduced the novel steam processing method, while focusing on shape memory and polymeric changes. The stress vs. strain response of the foam was not reported, neither before nor after conversion, nor were details of how to create the steam environment. If simple methods such as steam conversion [57] can produce closed cell auxetic foam with Young's moduli close to foam in protective equipment, prosthetics and footwear, auxetic foams could be developed for these applications. This work explores the steam conversion method for auxetic closed cell foam, and its effect on Young's modulus and Poisson's ratio in more detail than previous work [57].

## **METHODS**

### **Foam conversion**

Cuboidal samples measuring  $100 \times 20 \times 10$  mm were cut with a Stanley knife from sheets of closed cell low density polyethylene (LDPE) foam (Plastazote LD-60, supplied by Algeos.com) with a skin to skin density of  $60 \text{ kg/m}^3$  [58]. LD-60 was selected following pilot testing where higher magnitude NPR was achieved than for other candidates (Plastazote LD-24 and Evazote EVA-50, supplied by Algeos.com). LD-60 also had similar Young's modulus ( $\sim 1$  to  $3 \text{ MPa}$  [58]) to foam used in impact and modelling studies of football shin and ankle protection ( $> 1 \text{ MPa}$

[48,59]) and polyethylene foam used in prosthetic devices [28]. Samples were placed in a ceramic container (300 x 200 x 100 mm) filled to ~80% with water at room temperature (~20°C). The container was wrapped in aluminum foil then heated in an oven at 105°C (MCP Tooling Technologies LC/CD, +/- 0.25°C) for between 1 and 6.5 hours (1, 3, 4, 4.5, 5, 5.5, 6, 6.5 hours, six samples for each conversion time). The temperature of 105°C was selected to bring the water to the boil. After heating, the foams were removed from the water (< 30 seconds) and cooled on a drying rack in air at room temperature for ~20 minutes, when they visibly shrank, almost instantaneously. Foams were stored in an environmental chamber (10% relative humidity, 20°C) for one week before conversion and for the duration of the study, following conversion. Testing was in an air-conditioned laboratory with an expected temperature of 20 to 25°C and relative humidity of 30 to 60%.

## **Measurements**

Sample dimensions and mass were recorded to see if foam water content and volume changed with time, after conversion. Following conversion, the center of the foam cuboids, where steam was trapped, reduced in volume more than the edges, which have open cells and cannot trap steam, leaving a concave cross sectional area [57]. Concave profiles were curved, becoming square as the FVR increased (Figure 1). Dimensions (Vernier Calipers with a resolution of 0.01 mm) and mass (Sartorius, M-power with a resolution of 0.1 mg) of all samples were recorded: i) before conversion, ii) ~16 hours after removal from the oven, and iii) every ~24 hours for the following week (i.e. 16, 30, 54 to 174 hours). To obtain sample cross-sectional areas and volumes, the depth of all concave profiles (h in Figures 1b and c) and the width of cuboidal concave profiles were measured (Figure 1c). Three samples were allocated for mechanical characterization after one week. The remaining three samples were re-measured a week later, at two weeks after conversion.

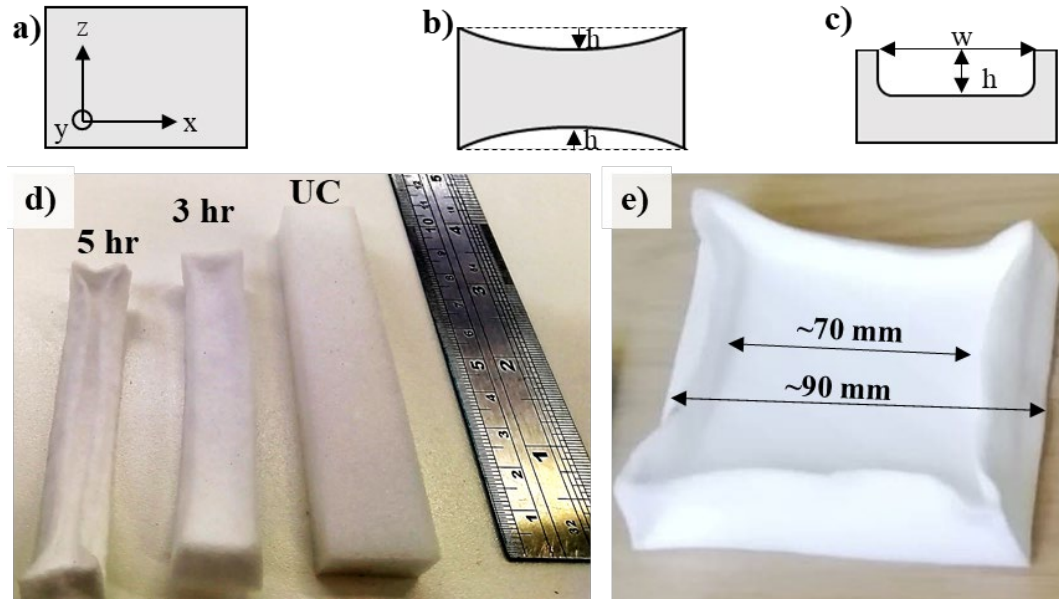


**Figure 1:** Schematic of a) unconverted, square cross sections, b) a cross section with curved concave profile, c) a cross section with a cuboidal concave profile, d) photo showing unconverted LD-60 sample (UC) and LD-60 samples converted for 3 and 5 hours, e) photo showing the larger converted sample (original dimensions 100 x 100 x 30 mm). Annotations  $h$  and  $w$  in b) and c) are the width and depth of concave profiles. Annotations in (e) show total width and width of the uniform thickness inner section. a) Shows coordinate system, with  $y$  parallel to sample length,  $z$  to thickness and  $x$  to width.

## Mechanical Characterization

One week after conversion, a speckle pattern was applied to the three samples allocated for mechanical characterization (Matt Acrylic Spray Paint, Halfords) to allow for full field strain measurement using digital image correlation (DIC), as per previous work [60–62]. Tensile samples were clamped (10 mm from each end, leaving 60 to 80 mm) in the test device jaws, which were closed to 1 mm, corresponding to between 10 and 20% of the original sample thickness, (Instron 3369, 500N load cell, Figure 2) and extended to 10% strain ( $0.0033 \text{ s}^{-1}$ ). One face of each sample was filmed for each test, so DIC could be undertaken (LaVision 3D DIC package, 1260 x 1080 p cameras, 10 fps, Nikon lenses with 60 mm optical zoom and two LED lights). A target area was set over the central lengthwise third of samples (Figure 2b), giving axial and lateral true strains, with facet sizes set to give a minimum of three speckles per facet (10 to 15 pixels) [63]. Samples

were rotated 90° about the loading (y, Figure 2b to c) axis after each test to record strains on all four faces during repeat testing.

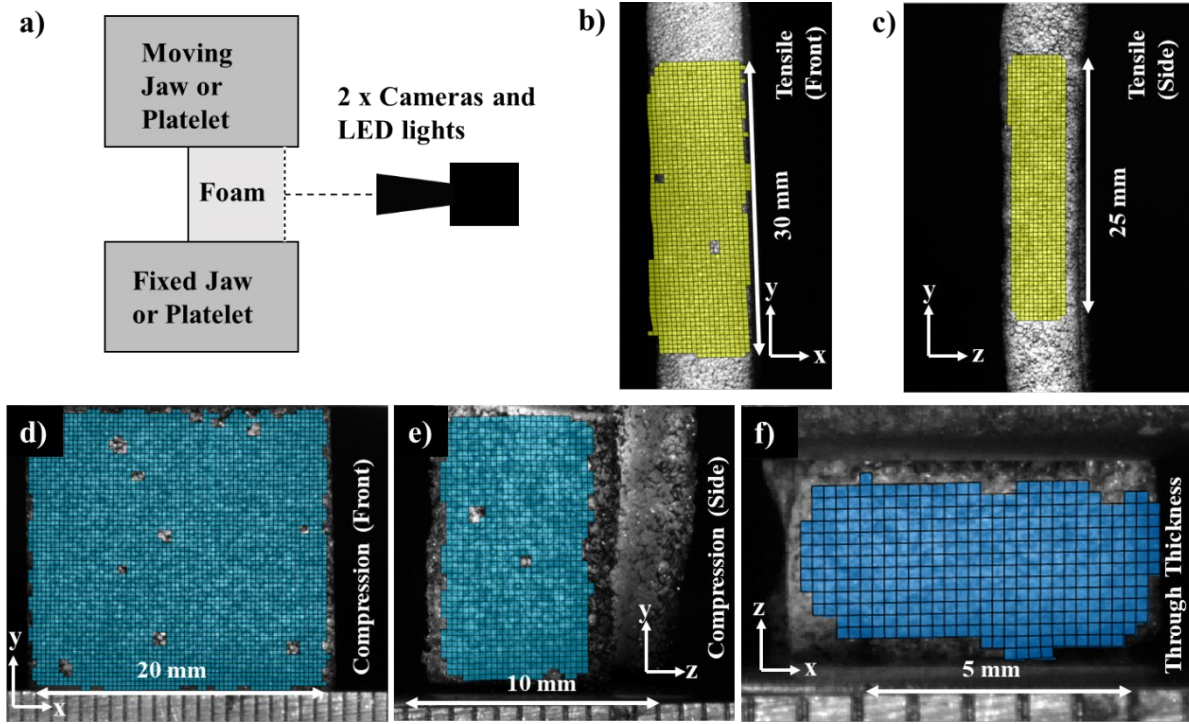


**Figure 2:** a) Schematic of mechanical test set up, and regions of interest applied to b) the front of an unconverted tensile sample, c) the side of a converted (4 hour) tensile sample, d) the front of an unconverted compression sample e) the side of a converted (4 hour) compression sample and f) the front of a converted (4 hour) sample, with non-uniform edges cut off, during through thickness compression. Dimensions marked on images are for scale.

Compression testing was to 10% strain using platelets, with the same Instron device, strain rate and DIC camera set up as the tensile tests. Following tensile testing, the center of samples were cut to be equal in length to sample width, allowing compression parallel to previous sample length. With the low thickness of the unconverted sheet (10 mm), compression sample thickness was lower than the recommended minimum of 20 mm in ASTM D3574 – 11 [64]. To maintain as large samples as possible, width and length were kept maximal and equal by cutting tensile samples along their length, so the thickness (z-axis, Figure 2e) of samples was half of their width (x-axis, Figure 2d) or length (y-axis, Figure 2d). DIC was used to check for buckling during compression



tests parallel to the y axis, as some samples had higher aspect ratios ( $y/z = 2$ ) than recommended for foam compression tests ( $\leq 0.75$ ) [64], but similar to those in previous tests of auxetic open cell foam [50,65]. Samples were rotated  $90^\circ$  about their loading axis (y, Figure 2d to f) after each test, so full field strain measurements could be obtained for the four faces not covered by compression platelets. Cutting cubes from samples that adopted a concave cross section during conversion (Figures 1b & c) allowed compressive loading parallel to their width (x) and thickness (z). Two compression tests were applied to each of the two remaining axes (x and z, Figure 1a), with a  $90^\circ$  rotation between repeats allowing the same DIC methods to be applied to two faces. For the unconverted samples, cubes were cut and tested in three directions; i) compression in z, y lateral, ii) compression in y, x lateral and iii) compression in x, z lateral.

Force data taken from the Instron software (Bluehill 4.0, sample frequency 25 Hz) and measurements of cross sectional area and length (Vernier Calipers) taken before each test were used to calculate engineering stress and strain. The concave cross sectional areas of some converted samples were accounted for during stress calculations, as with previous volume measurements (Figure 1). The gradient of linear trend lines fitted to stress vs. axial strain plots gave Young's modulus up to 1% axial strain. Original length in strain calculations was the height of compression samples and the gauge length (distance between grips) for tensile samples. Poisson's ratio was the negative product of the gradient of linear trend lines fitted to axial vs. transverse true strain (from DIC), up to 1% axial strain. Comparisons of mean axial strain across the target area from DIC (Figure 2) and applied strain (10%) after each test showed reasonable agreement ( $\pm 3\%$  strain).

## **Micro-CT**

Micro-computed tomographic scans were collected (SkyScan 1172; 180° rotation, image acquisition every 0.7°, resolution < 5 µm) for unconverted foam, and the samples of foam steamed for 3 and 6.5 hours, selected to give a range of FVRs between 1.0 and 4.5. Micro-CT data were rendered (SkyScan, CTVox) and images of one cell or ~300 to 500 µm deep volumes and 5 µm cross sections recorded to compare cellular structures and identify any damage or ruptures to cell walls.

### **Larger samples**

Following investigation of the steam processing method using the small samples outlined above, larger samples (~100 x 100 x 30 mm) of the same foam (Plastazote LD-60, supplied by Advanced Seals and Gaskets, UK) were also converted. These larger samples were steamed for 8 hours using the method described previously, and stored in the environment chamber (10% relative humidity, 20 °C) after conversion and between tests. Conversion time was increased above the longest duration of 6.5 hours used for the smaller samples, following pilot testing where the larger foam sample did not shrink enough. Sample measurements (Vernier Calipers) and masses (Sartorius, M-power) were taken before and seven days after conversion to obtain linear compression ratios (LCR, final/original dimension) in each axis, and FVR. LCRs were approximated across the center of the converted sample (Figure 1e), minimizing the effect of the concave, uncompressed edges.

Three samples (~10 x 10 x 70 mm) were cut from the central regions (30 x 70 x 10 mm) of the converted cuboid for mechanical characterization, with the longest dimension parallel to the y-axis, and were also weighed and measured. The concave, uncompressed edges formed in smaller samples (Figure 1) and present around the outer ~10 mm of the converted cuboid (Figure 1e) were removed before tensile samples were cut. Mechanical characterization followed the protocol used for the samples converted from smaller cuboids. As with the unconverted foam in previous tests,

cubes were cut from the center of cuboidal tensile samples for compression testing in three directions; i) compression in y, z lateral, ii) compression in z, x lateral and iii) compression in x, y lateral; with the z direction being through-thickness and x and y being both planar directions.

## RESULTS

### Small cuboids (10 x 20 x 100 mm)

Following steam conversion, sample mass returned to, then remained, within 0.2% of its original value after a week. FVR increased when samples were removed from the steaming environment, contracting within 1 to 2 minutes, and then typically reduced slightly or remained relatively unchanged over time, again settling after a week. The unconverted foam samples, cut from the center of a larger one by the supplier, had a lower density ( $51 \text{ kg/m}^3$ ) than the value in the supplier's data sheet ( $60 \text{ kg/m}^3$ ) [58]. Sample density increased after conversion, due to the decrease in volume (Figure 3) rather than increased mass caused by moisture uptake; mass had returned to within 0.2% of its original value after two weeks, when density was calculated (Figure 3a). FVR tended to increase with conversion time, with values exceeding four for samples steamed for 5 hours or more (Figure 3b). Samples converted for 4.5 hours were outliers.

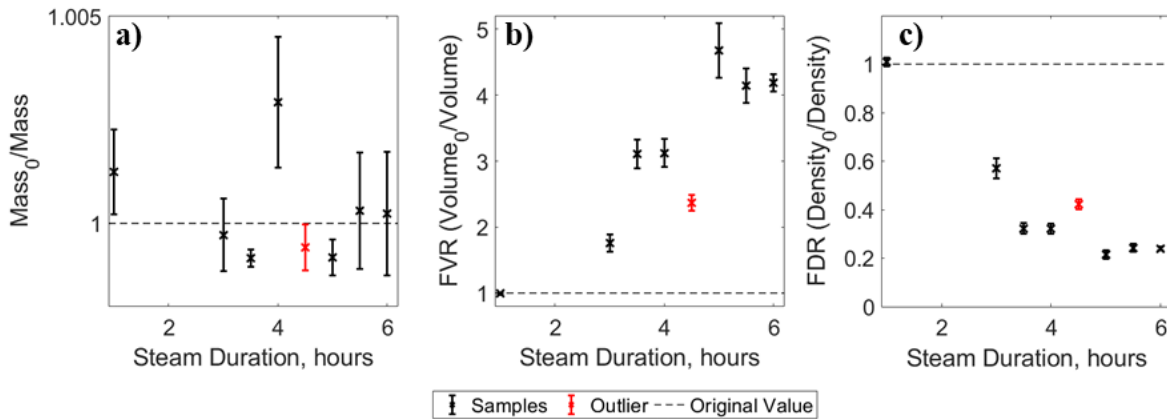


**Figure 3:** Mean a) Original/final mass, b) FVR and c) FDR two weeks after conversion, for each conversion time. Error bars show 1 standard deviation, outlying sample shown in red

As FVR increased with conversion time, the regular cellular structure of the foam (Figure 4a) became more contorted, and the angles between cell walls became more re-entrant (Figure 4b & c). In the volume renderings, cell walls other than those perpendicular to the field of view appear transparent. Ruptures to cell walls were not seen in the 5  $\mu\text{m}$  thick cross sections (Figure 4 inserts), suggesting they remained intact. Cell rise (anisotropic elongation) was not visible in the unconverted foam (Figure 4a).

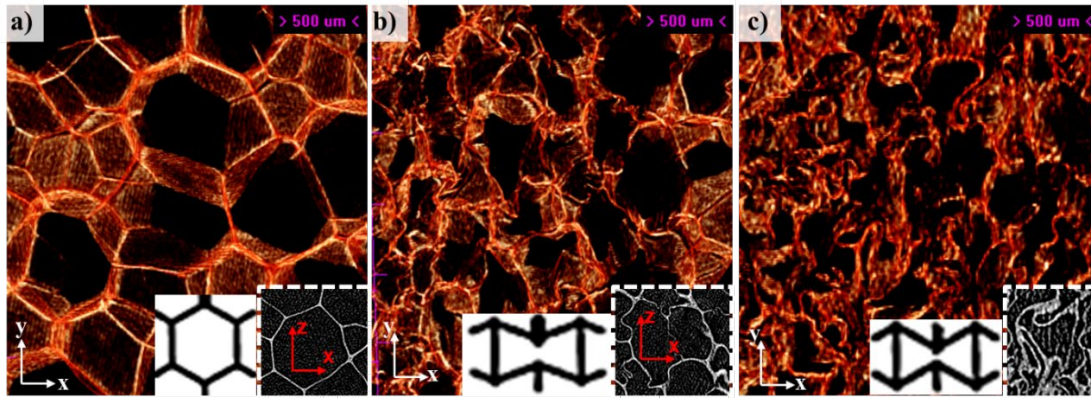


**Figure 4:** Rendered volumes of Micro-CT scans at a depth of 300 to 500  $\mu\text{m}$  (one cell) of; a) Unconverted foam and foam converted for a) 3 and b) 6.5 hours, with respective FVRs of 1.74 and 4.42. Inserts show 5 micrometer thick cross sections, labels show orientation (Figure 1), other than in c (same as in b & c). Schematics of 2D projections of cells show how changes to FVR and cell size, as a result of changing angles between cell walls.

Contour plots of transverse strain from DIC (Figure 5) show the unconverted foam expanded and the converted foam contracted during compression, indicating respective positive and negative Poisson's ratios. Figure 5b shows a side view of a sample with a high aspect ratio ( $y/z = 2$ ) compressing along its long y-axis with straight edges, without buckling in its shorter z-axis. Lateral vs. compressive axial strain was nonlinear, varying with applied strain (Figure 6). Compressive lateral vs. axial strain plots (Figure 6) for unconverted and converted samples show an initial increase in gradient and Poisson's ratio (up to 1% strain) with FVR; from positive Poisson's ratio expansion (UC / FVR = 1) to contraction and NPR (FVR = 1.7 & 4.6), and then an increase back

to near zero values for conversion times over 5 hours (FVR = 4.4). Tensile lateral vs. axial strain plots of converted foams (Figure 6) had a similar trend to compressive plots, with Poisson's ratio decreasing (from positive Poisson's ratio contraction to negative Poisson's expansion for samples converted for 3 hours), but then increasing to positive Poisson's ratio at longer conversion times ( $\geq 5$  hours).

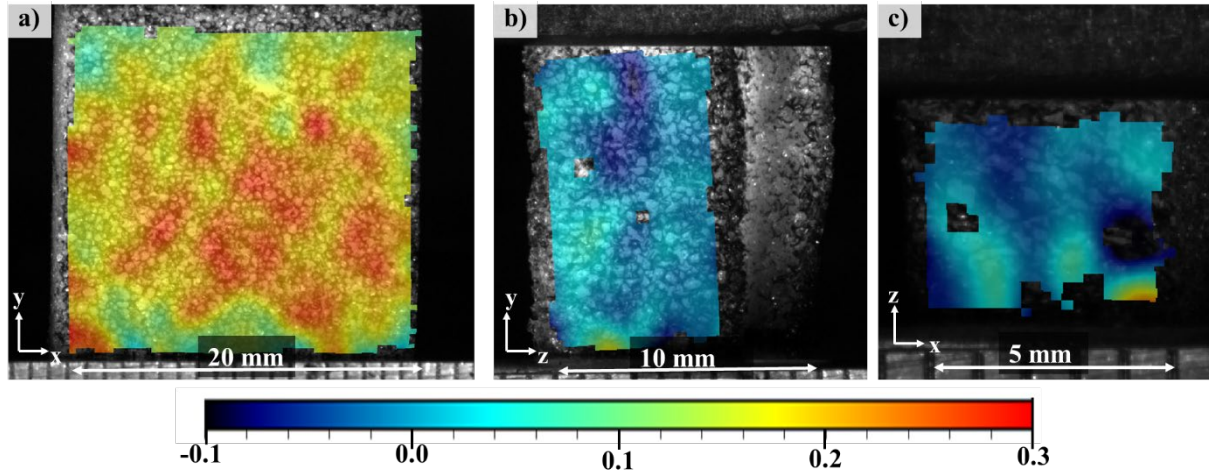


**Figure 5:** Contour plots of lateral strain at maximum compression from DIC for a) unconverted (front of sample), and foam converted for 5 hours 30 minutes with an FVR of 4.16, from the side during b) lengthwise compression and c) through thickness compression. Same scale for all (negative is contraction).

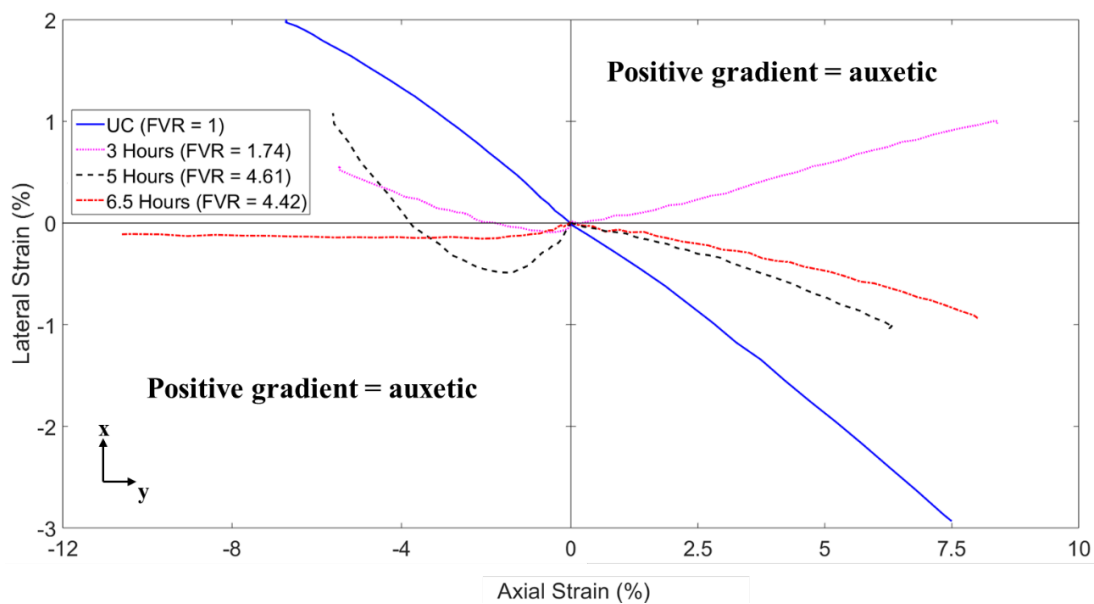


**Figure 6:** Lateral (x direction) vs axial (y directions) strain plots from DIC in compression and tension. Negative strain values indicate compression.

Unconverted foam exhibited Poisson's ratios (measured up to 1% strain) of  $0.34 \pm 0.01$  (Mean  $\pm$  S.D.) in compression and  $0.33 \pm 0.07$  in tension (Figure 7a & b), similar to previous tests of unconverted closed cell foam [56,57]. Compressive Poisson's ratios were negative for samples with FVRs between 1.8 and 4.6, with a maximum magnitude mean NPR of  $-0.11 \pm 0.03$  (Figure 7a), but NPR was generally only maintained to  $\sim 2\%$  compression (Figure 6). Tensile Poisson's ratios were negative for samples with FVRs between 2.4 and 4.4, with a maximum magnitude NPR of  $-0.07 \pm 0.15$ , (Figure 7b), and relatively linear over the tested region ( $\sim 8\%$  tension, Figure 6).

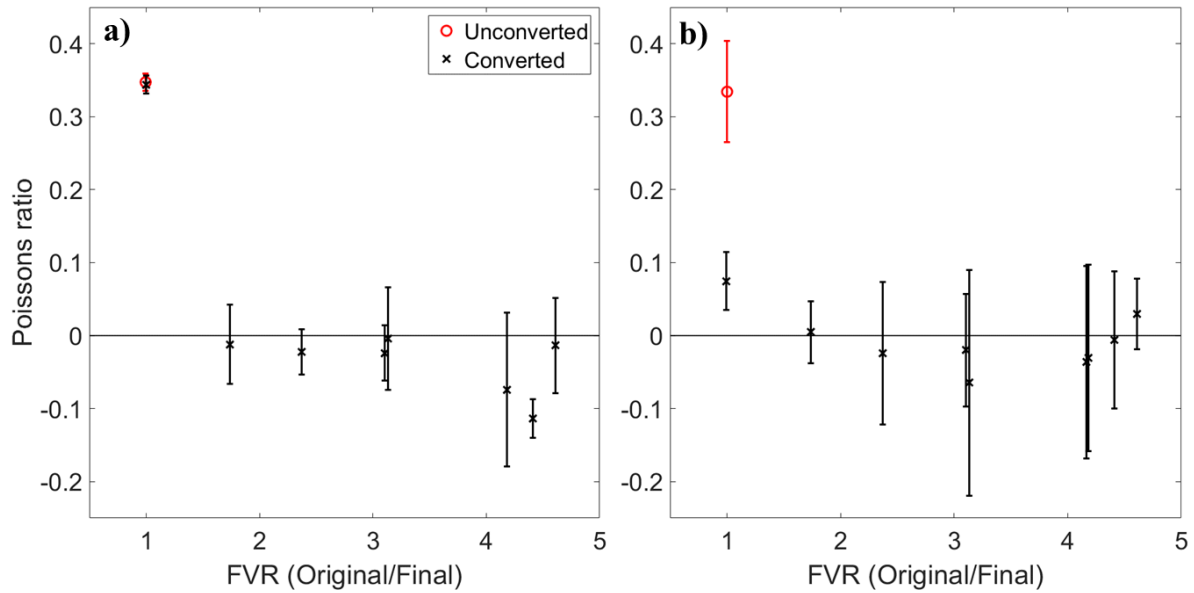


**Figure 7:** Poisson's ratio up to 1% axial strain vs FVR, in a) compression and b) tension. Same legend and y-axis for both a & b. Error bars show one standard deviation (all samples & orientations).

The gradient of compressive and tensile stress vs. strain plots, and therefore Young's modulus, mostly increased with conversion time and FVR (Figure 8). The stress vs. strain relationship for the unconverted sample exhibited a plateau and reduction in gradient around 5% compression (Figure 8). The plateau was present, but reduced, in the samples converted for 3 and 5 hours, but not present in those converted for over 5 hours.

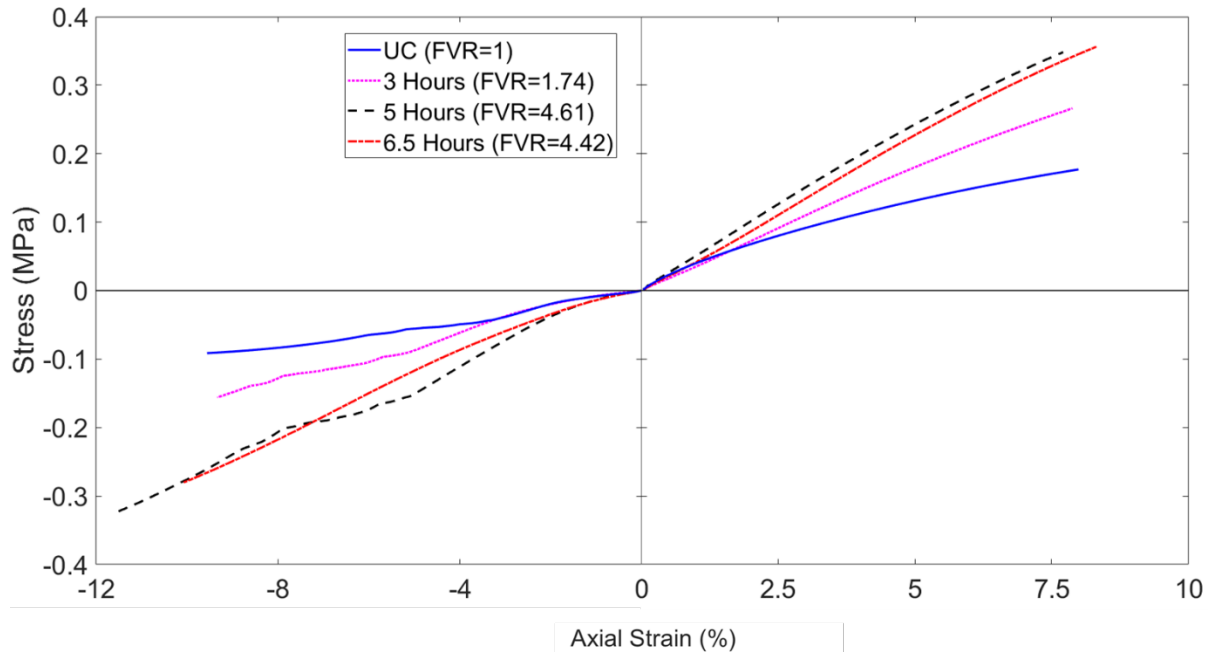


**Figure 8:** Stress vs axial strain during loading parallel to sample length (y-axis), from Instron data in compression and tension. Negative stress and strain values indicate compression.

In compression, samples with an FVR of one to three exhibited lower compressive Young's moduli (0.5 to 1 MPa, measured up to 1% strain) than their unconverted counterparts (~ 1.5 MPa), whereas samples with an FVR of 2.4 to 4.6 exhibited similar compressive Young's moduli (1 to 1.5 MPa) to the unconverted samples (Figure 9a). During compression, the Young's modulus of unconverted foam, and foam converted for 3 hours, decreased beyond ~2% compressive strain (Figure 8), exhibiting the plateau region of many conventional foams [46]. Tensile Young's moduli of samples with an FVR exceeding two increased with FVR from ~3 to 6 MPa (Figure 9b), and all tested samples exhibited quasi-linear stress vs. strain relationships (Figure 8).

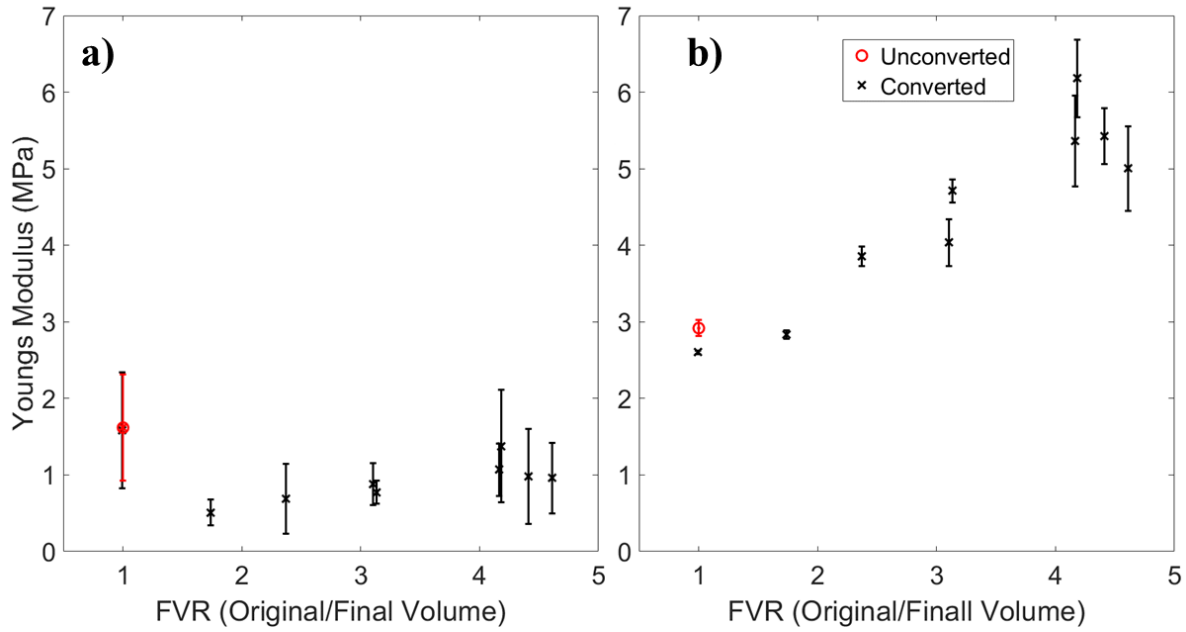


**Figure 9:** Young's modulus up to 1% axial strain vs FVR in a) compression and b) tension. Same legend and y-axis for both a & b. Error bars show one standard deviation (all samples & orientations).

### Large cuboid (30 x 100 x 100 mm)

The outer ~10 mm of the larger cuboid contracted less than the center during conversion (Figure 1e), as with smaller samples (Figures 1b & c). The ~70 x 70 x 10 mm (final dimensions) center of the converted cuboids compressed almost evenly with almost uniform thickness. The sample shrank slightly more than smaller samples converted for 3 hours, with an FVR of  $2.25 \pm 0.04$  (Table 1). The sample shrank more through its thickness (from 28 to ~11 mm, LCR = 0.39) than the other two axes (~100 to ~90 mm, LCR = 0.92) during conversion, which would be expected to cause higher re-entrant angles between cell walls in the z-x plane (Figure 10, Table 1). The unconverted foam had a density of  $61 \text{ kg/m}^3$  before conversion, similar to the value of  $60 \text{ kg/m}^3$  in the supplier's data sheet [58].



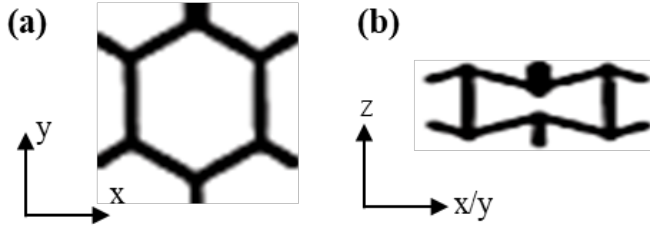


**Figure 10:** Schematics assumed from LCR, showing 2D projections of cell shapes for the large cuboid in a) the y-x plane with relatively little compression ( $LCR_x$  and  $LCR_y \approx 0.9$ ), and; b) the z-x/y planes, with high through thickness compression ( $LCR_z$  of  $\approx 0.4$ ).

All tested samples had NPR in tension and compression (Figure 11a, Table 1); when either transverse deformation or axial loading were parallel to sample thickness (z-axis). The magnitude of NPR was highest when loading was parallel to the longer cell y-axis (Figure 10b), and transverse expansion was through thickness ( $v_{yz}$ , Figure 11a and Table 1); -0.33 up to 10% tension and -1.07 up to 1% compression, then becoming positive (Figure 11a). With similar LCRs of 0.9 in both planar dimensions,  $v_{xz}$  would be expected to be similar to  $v_{yz}$ . Poisson's ratios during compression parallel to the z-axis were negative or near zero (-0.01), but almost constant to  $\sim 10\%$  compression (Figure 11a). Poisson's ratios were positive (tensile  $v_{yx} = 0.18$  and compressive  $v_{xy} = 0.21$ ) in both planar directions (Figure 11a, Table 1), which had compressed less following steaming, meaning cell shapes would be expected to be more similar to those of the unconverted foam (Figure 10a). Stress vs. strain relationships of the converted samples were quasi-linear (Figure 11b). As with the smaller samples with an FVR of  $\sim 2$  (Figure 9a), the compressive Young's moduli remained almost unchanged or decreased following conversion; reducing from  $\sim 1.5$  to  $0.5$  MPa during through thickness compression, but increased to  $\sim 4$  MPa in tension (Table 1).

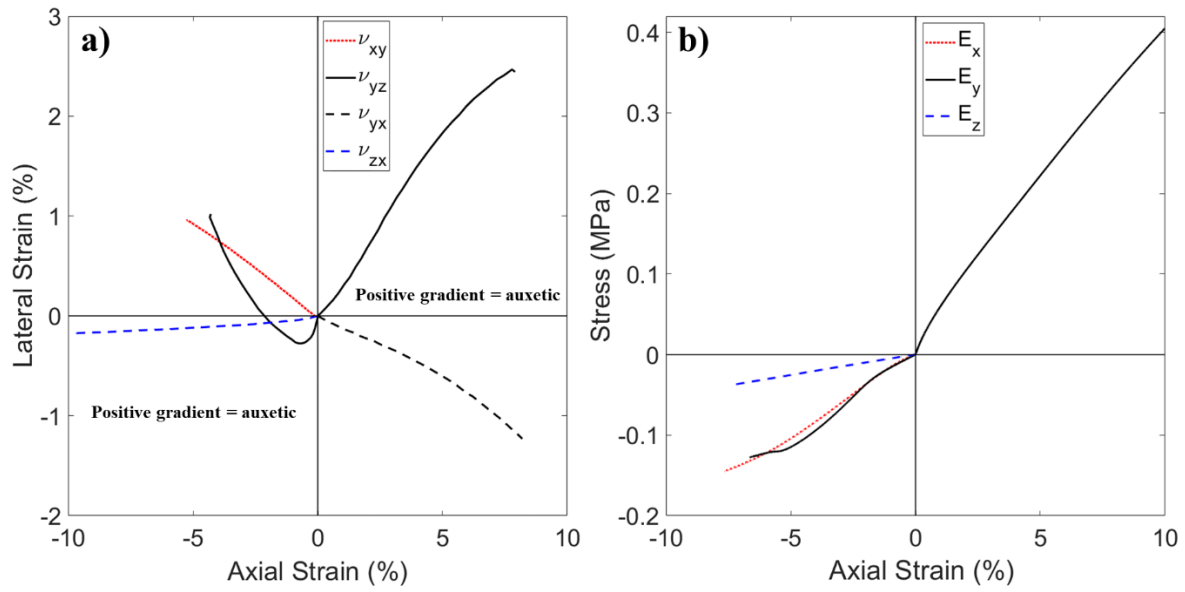


**Figure 11:** a) Lateral stress vs. axial strain, and; b) axial stress vs. axial strain plots for tests of the same samples cut from the larger sheets, in all tested orientations. Negative strains and stresses correspond to compression, or lateral contraction.

**Table 1:** Properties of the ~90 x 90 x 10 mm converted cuboid.

		Mean	S.D.
<b>Measurements</b>	Density - kg/m <sup>3</sup>	129.30	9.87
	FVR	2.25	0.04
	LCR <sub>xy</sub>	0.92	0.00
	LCR <sub>z</sub>	0.39	0.08
<b>Young's Moduli</b>	T E <sub>y</sub> (Mpa - 0-10 %)	3.86	0.06
	C E <sub>y</sub> (Mpa - 0-10 %)	2.21	0.28
	C E <sub>z</sub> (Mpa - 0 -10 %)	0.52	0.03
	C E <sub>x</sub> (Mpa - 0-10 %)	1.46	0.57
<b>Poisson's Ratios</b>	T $\nu_{yx}$ (0-10 %)	0.18	0.03
	T $\nu_{yz}$ (0-10 %)	<b>-0.33</b>	<b>0.03</b>
	C $\nu_{yz}$ (0-1 %)	<b>-1.07</b>	<b>0.37</b>
	C $\nu_{zx}$ (0-1 %)	<b>-0.01</b>	<b>0.01</b>
	C $\nu_{xy}$ (0-1 %)	0.21	0.11

## DISCUSSION

The FVR of closed cell auxetic foam tended to increase with conversion time when using the steam conversion method (Figure 3b). One set of samples converted for 4.5 hours had lower than expected FVR, caused by a tear in the covering foil during conversion. Future work could use a dish with a sealed lid. For the small samples (original dimensions 100 x 20 x 10 mm), compressive Young's moduli were lower than tensile; decreasing from  $\sim 1.5$  MPa as the compressive stress plateau became less prominent (Figure 9a, FVR between 1 and 2), then increasing with FVR to reach a limit below 2 MPa and FVR above 3 (Figure 9a). Some of the compression samples were smaller, or had higher aspect ratios ( $y/z$ ) than specified in ASTM D3574 – 11, although the standard was followed as closely as possible [64]. Further work converting and testing larger samples would make it easier to extract samples for testing that adhere to relevant standards, and may reduce experimental variation. Tensile Young's moduli increased with FVR (Figure 9b) and remained quasi-linear with applied strain (Figure 8).

For the smaller cuboids, the highest magnitude tensile NPRs (of -0.07) were achieved with FVRs from 2.4 to 4.6 (Figure 8), following steam processing for 3 to 6.5 hours (Figure 3b). This range of FVRs that produced the highest magnitudes of tensile NPRs were similar to those reported in previous work making closed cell auxetic foam (two to five [56,57]). However, the mean, maximum magnitude tensile and compressive NPR of these small samples were lower ( $\sim -0.1$ , Figure 7) than tensile Poisson's ratios measured in previous work converting larger samples with a similar procedure ( $\nu \approx -0.5$  [57]), or applying more even compression to 2 cm sided cubes in a pressure vessel ( $\nu \approx -2.0$  [56]). Poisson's ratio increased and became positive beyond  $\sim 5\%$  compression, but remained negative and almost constant to  $\sim 10\%$  tension (Figure 6).

As in previous work [57], samples shrank less towards their outer surface. Steam condensation could not produce a negative pressure differential at the outer surfaces of the sample, because cells

faces were cut and effectively open, resulting in a concave cross section (Figure 1). The cross section of all tested samples was uniform along the loading axis during tension and compression tests, so would not have affected Young's modulus measurements. Using 3D, rather than 2D, DIC can account for differences in full field strain measurement for curved faces [66]. When converting the larger cuboid (100 x 100 x 30 mm), only the outer ~10 mm planar edges were less compressed and hence concave; the inner ~70 mm were of almost uniform thickness (of ~11 mm). Through thickness compression of larger cuboids during conversion was greater than planar compression (Table 1). With fewer non-shrinking cells constraining through thickness compression, the larger cuboid had greater magnitude (anisotropic) NPR (-0.3 in tension, -1.1 in compression, Table 1) than the smaller samples (Figure 8), and similar values to previous work using the same steam processing method on different foam [57]. Anisotropy was related to the shape of the unconverted samples, and converting cubes rather than cuboids may produce isotropic samples. For impact protection, the through thickness characteristics, including NPR and stiffness, are thought to be most important [6]. Further work could look to fabricate auxetic foam with higher magnitude through thickness NPR (above -0.01, Table 1), by converting cubes, adjusting processing time, and exploring other candidate foams. The influence of oven temperature on steam conversions could be a topic for future work, particularly when converting foams with softening points much higher than 100 °C.

The range of Young's moduli imparted (0.5 to 6 MPa, Table 1 and Figure 9), and a plateau in stress vs. strain relationships (Figure 8), are useful for sporting protective equipment [9,20,48]) and prosthesis socket liners [26–28]. Foam in protective equipment has a similar Young's modulus to foam fabricated herein; selected to deform at stresses below, or at the lower end of, those which cause soft tissue damage such as bruising, in the order of 1 to 10 MPa [67,68]. Auxetic open

cell foam typically has a low Young's moduli between  $\sim 0.02$  and  $0.20$  MPa [10,44,49,50], and previous auxetic closed cell foam had a high Young's moduli between  $\sim 50$  to  $250$  MPa [56], each far from the injury threshold range. Foam in protective devices typically has a stress plateau between  $\sim 5$  and  $80\%$  compression [48,51,69], which can be used to ensure energy absorption continues as foam compression increases, while keeping pressure, force, or acceleration below an injury threshold value. Preserving the compressive stress plateau region in auxetic foam is, therefore, likely to be useful (Figure 8).

Through inspection of micro-ct data, neither ruptured cell walls [33,47] nor cell rise direction [46] were observed in the converted or unconverted samples (Figure 4). No pressure differential nor contraction would occur within ruptured or open cells; evidenced by cells on the outer surface not contracting. Based upon the visually evident and measured (Figures 1 & 3, Table 1) volumetric compression, and backed up with increasing tangent moduli and micro-ct data, the converted auxetic foam's closed cells were probably intact.

Increasing FVR increased the prevalence and angle of re-entrant walls (Figure 4b & c). Analytical models for cell rib, flexure and hinging of open cell foam [46,70] predict the increase in Young's modulus with increasing FVR, and re-entrant angle between cell walls, evident in Figure 9. These models also predict the initial increase in the magnitude of NPR with FVR and re-entrant cell wall angle, followed by the plateau for  $FVR > 3$ , evident in Figure 7. Considering the larger, anisotropic converted cuboid, the positive Poisson's ratio and similar stiffness to the unconverted foam observed in the x-y plane was as expected; with LCRs of  $\sim 0.9$  and relatively little change to cell shape or mechanical properties. Work stretching open cell foam during thermo-mechanical conversions [41], and analytical models [46,70], predict higher stiffness parallel to the foam long cell axis; agreeing with the higher  $E_x$  and  $E_y$  than  $E_z$  (Table 1). Symmetric compliance

of orthotropic materials such as these, whereby  $E_y \times v_{zy} = E_z \times v_{yz}$  [71], and analytical foam models [46,70], then predict a high magnitude  $v_{yz}$ , based on the low  $E_z$  and high  $E_y$ . Further modelling work, based on three-dimensional reconstructions of micro-ct data, and considering the effect of gas pressure on cellular mechanics [69], could further clarify the effect of cell shape on mechanical properties.

This work, fabricating closed cell foams of comparable stiffness and sizes to foam sheets in sporting and other protective equipment, paves the way for application based impact testing of closed cell foam sheets and prototype protective pads and equipment. Impact tests could follow standards for protective equipment (e.g. EN13061 for football shin pads [72]), and more closely replicate infield condition, by using biofidelic anvils and testing at different temperatures and relative humidities [73]. We recommended that the compressive stiffness of specific products is first matched (e.g.  $\sim 1$  MPa for a football shin pad [48,59] or prosthesis socket liner [26–28]). For the small cuboids, Young's modulus was close to 1 MPa for FVRs between 2 and 4 (Figure 9a), following 3 to 5 hour conversions. For the larger samples, the 8 hour conversion produced foam with an FVR close to two but low through thickness Young's modulus ( $E_z$ ) of 0.5 MPa (Table 1), and these values may perhaps be increased by a longer steaming time. Comparing auxetic and conventional foam samples with equivalent stress vs. strain relationships will determine the effect of NPR; expected to decrease the likelihood of penetration by concentrated loads [1,2,74], decrease peak impact forces [4,6,7], increase vibration damping [3] and increase conformability [9,75].

## CONCLUSIONS

FVR and cell reentrancy increased (from 1.3 to 4.6) for small samples (10 x 20 x 100 mm) of closed-cell foam with the duration of steam conversion (between 1 and 6.5 hours). Cells on the outer surface of the foam did not contract during conversion; resulting in non-uniform shapes in

small samples. Larger cuboids with 100 mm sides and 30 mm thickness shrank more evenly following conversion than the smaller cuboids (100 x 20 x 10 mm), so larger samples may be better suited to producing closed cell auxetic foam with the steam conversion method. Sample mass returned to its original value three days after conversion, suggesting absorbed water had left the samples. Tensile and compressive Young's modulus of all foams first decreased then increased (ranging from ~0.5 to ~6.0 MPa) with FVR, which were between about two and five. NPRs as low as -1.07 up to 1% compression, and -0.33 up to ~10% tension were obtained. This work further demonstrates the simplicity and potential of the steam conversion method, and its effects on Young's modulus and Poisson's ratio, paving the way for further application based testing of auxetic closed cell foam for protective devices, prosthetics and footwear.

### **Acknowledgements**

The research was funded by Sheffield Hallam University, through the Creating Knowledge Investment Platform, and Manchester Metropolitan University, through the Strategic Opportunities Fund. Alana Birch contributed to foam conversion, testing and analysis while on a Nuffield Research Placement at Manchester Metropolitan University. The manuscript was written through contributions of all authors. All authors have given approval to the final version of the manuscript. Olly Duncan carried out the work with the help of Alana Birch; Tom Allen and Andrew Alderson gave in depth feedback and advice; Leon Foster and John Hart gave advice when asked.

### **REFERENCES**

1. Allen T., Duncan O., Foster L., Senior T., Zampieri D., Edeh V., et al. Auxetic foam for snow-sport safety devices. *Snow Sport. Trauma Saf. Proc. Int. Soc. Ski. Saf.* **2016**.21.
2. Chan N., Evans K.E. Indentation resilience of conventional and auxetic foams. *J. Cell. Plast.* **1998**.34. 231–60.

3. Scarpa F., Giacomini J., Zhang Y., Pastorino P. Mechanical performance of auxetic polyurethane foam for antivibration glove applications. *Cell. Polym.* **2005**.24(5). 253–68.
4. Allen T., Shepherd J., Hewage T.A.M., Senior T., Foster L., Alderson A. Low-kinetic energy impact response of auxetic and conventional open-cell polyurethane foams. *Phys. Status Solidi Basic Res.* **2015**.9. 1–9.
5. Duncan O., Foster L., Senior T., Alderson A., Allen T. Quasi-static characterisation and impact testing of auxetic foam for sports safety applications. *Smart Mater. Struct.* **2016**.25(5). 054014.
6. Ge C. A comparative study between felted and triaxial compressed polymer foams on cushion performance. *J. Cell. Plast.* **2013**.49(6). 521–33.
7. Lisiecki J., Błazejewicz T., Kłysz S., Gmurczyk G., Reymer P., Mikułowski G. Tests of polyurethane foams with negative Poisson's ratio. *Phys. Status Solidi Basic Res.* **2013**.250(10). 1988–95.
8. Evans K.E. The design of doubly curved sandwich panels with honeycomb cores. *Compos. Struct.* **1991**.17(2). 95–111.
9. Duncan O., Shepherd T., Moroney C., Foster L., Venkatraman P.D., Winwood K., et al. Review of auxetic materials for sports applications: Expanding options in comfort and protection. *Appl. Sci.* **2018**.8(6). 941.
10. Lakes R.S. Foam Structures with a Negative Poisson's Ratio. *Science* (80-. ). **1987**.235(4792). 1038–40.
11. Evans K.E., Alderson A. Auxetic materials: Functional materials and structures from lateral thinking! *Adv. Mater.* **2000**.12(9). 617–28.
12. Foster L., Peketi P., Allen T., Senior T., Duncan O., Alderson A. Application of Auxetic Foam in Sports Helmets. *Appl. Sci.* **2018**.8(3). 354.
13. Alderson A., Alderson K.L., McDonald S.A., Mottershead B., Nazare S., Withers P.J., et al. Piezomorphic materials. *Macromol. Mater. Eng.* **2013**.298(3). 318–27.
14. Sanami M., Alderson A., Alderson K.L., McDonald S. a., Mottershead B., Withers P.J. The production and characterization of topologically and mechanically gradient open-cell thermoplastic foams. *Smart Mater. Struct.* **2014**.23(5). 055016.
15. Stojmanovski Mercieca L.A., Formosa C., Grima J.N., Chockalingam N., Gatt R., Gatt A. On the Use of Auxetics in Footwear: Investigating the Effect of Padding and Padding Material on Forefoot Pressure in High Heels. *Phys. Status Solidi Basic Res.* **2017**.254(12). 1–5.
16. Bailly N., Laporte J.D., Afquir S., Masson C., Donnadiou T., Delay J.B., et al. Effect of Helmet Use on Traumatic Brain Injuries and Other Head Injuries in Alpine Sport. *Wilderness Environ. Med.* **2018**.29(2). 151–8.



17. Whyte T., Stuart C.A., Mallory A., Ghajari M., Plant D.J., Siegmund G.P., et al. A Review of Impact Testing Methods for Headgear in Sports: Considerations for Improved Prevention of Head Injury Through Research and Standards. *J. Biomech. Eng.* **2019**.141(7). 070803.
18. Mez J., Daneshvar D.H., Kiernan P.T., Abdolmohammadi B., Alvarez V.E., Huber B.R., et al. Clinicopathological Evaluation of Chronic Traumatic Encephalopathy in Players of American Football. *J. Am. Med. Assoc.* **2017**.02118(4). 360–70.
19. Prat N.J., Daban J.L., Voiglio E.J., Rongieras F. Wound ballistics and blast injuries. *J. Visc. Surg.* **2017**.154. 1–4.
20. Signetti S., Nicotra M., Colonna M., Pugno N.M. Modeling and simulation of the impact behavior of soft polymeric-foam-based back protectors for winter sports. *J. Sci. Med. Sport.* **2018**.
21. Schmitt K.U., Liechti B., Michel F.I., Stämpfli R., Brühwiler P.A. Are current back protectors suitable to prevent spinal injury in recreational snowboarders? *Br. J. Sports Med.* **2010**.44(11). 822–6.
22. Michel F.I., Schmitt K.U., Liechti B., Stämpfli R., Brühwiler P. Functionality of back protectors in snow sports concerning safety requirements. *Procedia Eng.* **2010**.2(2). 2869–74.
23. Lieberman D.E., Venkadesan M., Werbel W.A., Daoud A.I., Dandrea S., Davis I.S., et al. Foot strike patterns and collision forces in habitually barefoot versus shod runners. *Nature.* **2010**.463(7280). 531–5.
24. Relph N., Greaves H., Armstrong R., Gichuru P., Prior T.D., Griffiths I.B., et al. Running shoes for preventing lower limb running injuries in adults. *Cochrane Database Syst. Rev.* **2019**.2019(7).
25. Payne T., Mitchell S., Halkon B., Bibb R. A systematic approach to the characterisation of human impact injury scenarios in sport. *BMJ Open Sport Exerc. Med.* **2016**.2(1). e000017.
26. Armitage L., Rajan G., Kark L., Simmons A., Prusty B.G. Simultaneous measurement of normal and shear stress using fiber bragg grating sensors in prosthetic applications. *IEEE Sens. J.* **2019**.19(17). 7383–90.
27. Ali S., Abu Osman N.A., Naqshbandi M.M., Eshraghi A., Kamyab M., Gholizadeh H. Qualitative study of prosthetic suspension systems on transtibial amputees' satisfaction and perceived problems with their prosthetic devices. *Arch. Phys. Med. Rehabil.* [Internet]. **2012**.93(11). 1919–23. Available from: <http://dx.doi.org/10.1016/j.apmr.2012.04.024>
28. Sanders J.E., Daly C.H. How does vacuum forming affect Pelite mechanical properties? *Prosthet. Orthot. Int.* **1994**.18(1). 43–8.
29. Toronjo A. Articles of apparel including auxetic materials (US 20140059734 A1). Vol. 1. 2014.
30. Cross T.M., Hoffer K.W., Jones D.P., Kirschner P.B., Meschter J.C. Auxetic Structures And

Footwear With Soles Having Auxetic Structures (US 2015/0075034 A1). Vol. 1. 2015.

31. Bliven E., Rouhier A., Tsai S., Willinger R., Bourdet N., Deck C., et al. Evaluation of a novel bicycle helmet concept in oblique impact testing. *Accid. Anal. Prev.* **2019**.124(November 2018). 58–65.
32. Siegkas P., Sharp D.J., Ghajari M. The traumatic brain injury mitigation effects of a new viscoelastic add-on liner. *Sci. Rep.* **2019**.9(1). 1–10.
33. Chan N., Evans K.E. Fabrication methods for auxetic foams. *J. Mater. Sci.* **1997**.32. 5945–53.
34. Li S., Al-Badani K., Gu Y., Lake M., Li L., Rothwell G., et al. The Effects of Poisson's Ratio on the Indentation Behavior of Materials With Embedded System in an Elastic Matrix. *Phys. Status Solidi Basic Res.* **2017**.254(12). 1–8.
35. Choi J.B., Lakes R.S. Nonlinear properties of polymer cellular materials with a negative Poisson's ratio. *Mater. Sci.* **1992**.27. 4678–84.
36. Bianchi M., Scarpa F., Smith C.W. Shape memory behaviour in auxetic foams: Mechanical properties. *Acta Mater.* **2010**.58(3). 858–65.
37. McDonald S.A., Ravirala N., Withers P.J., Alderson A. In situ three-dimensional X-ray microtomography of an auxetic foam under tension. *Scr. Mater.* **2009**.60(4). 232–5.
38. Alderson A., Rasburn J., Evans K.E. Mass transport properties of auxetic (negative Poisson's ratio) foams. *Phys. Status Solidi - Basic Solid State Phys.* **2007**.244(3). 817–27.
39. Chan N., Evans K.E. The mechanical properties of conventional and auxetic foams. Part I: compression and tension. *J. Cell. Plast.* **1999**.35(2). 130–65.
40. Scarpa F., Yates J.R., Ciffo L.G., Patsias S. Dynamic crushing of auxetic open-cell polyurethane foam. *Proc. Inst. Mech. Eng. Part C J. Mech. Eng. Sci.* **2002**.216(12). 1153–6.
41. Alderson A., Davies P.J., Alderson K.I.M.L., Smart G.M. The Effects of Processing on the Topology and Mechanical Properties of Negative Poisson's Ratio Foams. *Proc. IMECE2005 2005 ASME Int. Mech. Eng. Congr. Expo. Proc. IMECE200*. **2005**. 1–8.
42. Grima J.N., Attard D., Gatt R., Cassar R.N. A novel process for the manufacture of auxetic foams and for their re-conversion to conventional form. *Adv. Eng. Mater.* **2009**.11(7). 533–5.
43. Li Y., Zeng C. Room-Temperature, Near-Instantaneous Fabrication of Auxetic Materials with Constant Poisson's Ratio over Large Deformation. *Adv. Mater.* **2016**.28(14). 2822–6.
44. Duncan O., Clegg F., Essa A., Bell A.M.T., Foster L., Allen T., et al. Effects of Heat Exposure and Volumetric Compression on Poisson's Ratios, Young's Moduli, and Polymeric Composition During Thermo-Mechanical Conversion of Auxetic Open Cell Polyurethane Foam. *Phys. Status Solidi.* **2019**.

45. Bianchi M., Scarpa F., Banse M., Smith C.W. Novel generation of auxetic open cell foams for curved and arbitrary shapes. *Acta Mater.* **2011**.59(2). 686–91.
46. Gibson L.J., Ashby M.F. Cellular solids. Structure and properties. **1997**.pp.67, 176–183, 259–264, 286, 301, 498p.
47. Mohsenizadeh S., Ahmad Z., Alipour R., Majid R.A., Prawoto Y. Quasi Tri-Axial Method for the Fabrication of Optimized Polyurethane Auxetic Foams. *Phys. Status Solidi.* **2019**.1800587. 1800587.
48. Ankrah S., Mills N.J. Performance of football shin guards for direct stud impacts. *Sport. Eng.* **2003**.6(4). 207–19.
49. Chan N., Evans K.E. The Mechanical Properties of Conventional and Auxetic Foams. Part II: Shear. *J. Cell. Plast.* **1999**.35. 166–83.
50. Boba K., Bianchi M., McCombe G., Gatt R., Griffin A.C., Richardson R.M., et al. Blocked shape memory effect in negative Poisson's ratio polymer metamaterials. *ACS Appl. Mater. Interfaces.* **2016**. acsami.6b02809.
51. Mills N.J., Fitzgerald C., Gilchrist A., Verdejo R. Polymer foams for personal protection: Cushions, shoes and helmets. *Compos. Sci. Technol.* **2003**.63(16). 2389–400.
52. Mills N.J., Gilchrist A. Modelling the indentation of low density polymer foams. *Cell. Polym.* **2000**.19(6). 389–412.
53. Verdejo R., Mills N.J. Heel-shoe interactions and the durability of EVA foam running-shoe midsoles. *J. Biomech.* **2004**.37(9). 1379–86.
54. Mills N. Running shoe materials. In: Jenkins M, editor. *Materials in sports equipment*. Elsevier; **2003**. p. 65.
55. Sanders J.E., Greve J.M., Mitchell S.B., Zachariah S.G. Material properties of commonly-used interface materials and their static coefficients of friction with skin and socks. *J. Rehabil. Res. Dev.* **1998**.35(2). 161–76.
56. Martz E.O., Lee T., Lakes R.S., Goel V.K., Park J.B. Re-entrant transformation methods in closed cell foams. *Cell. Polym.* **1996**.15(4). 229–49.
57. Fan D., Li M., Qiu J., Xing H., Jiang Z., Tang T. Novel Method for Preparing Auxetic Foam from Closed-Cell Polymer Foam Based on the Steam Penetration and Condensation Process. *ACS Appl. Mater. Interfaces.* **2018**.
58. Zotefoams. Plastazote® LD60 Low Density Polyethylene Foam Product Information [Internet]. [cited 2019 Oct 30]. Available from: <https://www.zotefoams.com/wp-content/uploads/2016/03/LD60-December-2017.pdf>
59. Ankrah S., Mills N.J. Analysis of ankle protection in Association football. *Sport. Eng.* **2004**.7(1). 41–52.
60. Allen T., Hewage T., Newton-Mann C., Wang W., Duncan O., Alderson A. Fabrication of

- Auxetic Foam Sheets for Sports Applications. *Phys. Status Solidi Basic Res.* **2017**.1700596. 1–6.
61. De Almeida O., Lagattu F., Brillaud J. Analysis by a 3D DIC technique of volumetric deformation gradients: Application to polypropylene/EPR/talc composites. *Compos. Part A Appl. Sci. Manuf.* **2008**.39(8). 1210–7.
  62. Phillips N., Hassan G.M., Dyskin A., Macnish C., Pasternak E. Digital image correlation to analyze nonlinear elastic behavior of materials. *Proc. - Int. Conf. Image Process. ICIP.* **2018**.2017-Sept.
  63. Wang D., Diazdelao F.A., Wang W., Lin X., Patterson E.A., Mottershead J.E. Uncertainty quantification in DIC with Kriging regression. *Opt. Lasers Eng.* **2016**.78. 182–95.
  64. Annual Book of ASTM Standards. Standard Test Methods for Flexible Cellular Materials — Slab , Bonded , and Molded Urethane Foams. Annual Book of ASTM Standards 2008.
  65. Bezazi A., Scarpa F. Mechanical behaviour of conventional and negative Poisson's ratio thermoplastic polyurethane foams under compressive cyclic loading. *Int. J. Fatigue.* **2007**.29(5). 922–30.
  66. Schreier H.W., Orteu J.J., Sutton M.A. Image correlation for shape, motion and deformation measurements: Basic concepts, theory and applications. Boston: Springer-Verlag; **2009**.pp.322p.
  67. Crisco J.J.T., Hentel K.D., Jackson W.O., Goehner K., Jokl P. Maximal contraction lessens impact response in a muscle contusion model. *J. Biomech.* **1996**.29(10). 1291–6.
  68. Beiner J.M., Jokl P. Muscle contusion injuries: current treatment options. *J. Am. Acad. Orthop. Surg.* **2001**.9(4). 227–37.
  69. Mills N.J., Zhu H.X. The high strain compression of closed-cell polymer foams. *J. Mech. Phys. Solids.* **1999**.47(3). 669–95.
  70. Duncan O., Allen T., Foster L., Senior T., Alderson A. Fabrication, characterisation and modelling of uniform and gradient auxetic foam sheets. *Acta Mater.* **2017**.126. 426–37.
  71. Timoshenko S.P., Goodier J.N. Theory of Elasticity. 3rd ed. New York: McGraw-Hill, USA; **1970**.
  72. European Committee for Standardization. BS EN 13061:2009 Protective clothing — Shin guards for association football players — Requirements and test methods. BS EN: 13061:2009. **2009**.
  73. Payne T., Mitchell S., Halkon B., Bibb R., Waters M. Development of a synthetic human thigh impact surrogate for sports personal protective equipment testing. *Proc. Inst. Mech. Eng. Part P J. Sport. Eng. Technol.* **2016**.230(1). 5–16.
  74. Alderson K.L., Pickles A.P., Neale P.J., Evans K.E. Auxetic polyethylene: The effect of a negative Poisson's ratio on hardness. *Acta Metall. Mater.* **1994**.42(7). 2261–6.

75. Sanami M., Ravirala N., Alderson K., Alderson A. Auxetic materials for sports applications. *Procedia Eng.* **2014**.72. 453–8.